scientific reports

Check for updates

OPEN

Physiopathological effects of entrance versus distal spread-out Bragg peak on mouse spinal cord neurons

Filippo Torrisi[1], Francesco Paolo Cammarata[2,3]✉, Valentina Bravatà[2], Marco Calvaruso[2], Cristiana Alberghina[2,3], Anna Maria Pavone[4], Giada Petringa[3], Giuseppe Antonio Pablo Cirrone[3], Simona Denaro[4], Anna Gervasi[4], Simona D'Aprile[4], Nunzio Vicario[4], Emanuele Scifoni[5], Pietro Pisciotta[6], Giorgio Russo[2,3,7] & Rosalba Parenti[4,7]

Recent investigations into radiation-induced side effects have focused on understanding the physiopathological consequences of irradiation on late-responding tissues like the spinal cord, which can lead to chronic progressive myelopathy. Proton therapy, an advanced radiation treatment, aims to minimize damage to healthy tissues through precise dose deposition. However, challenges remain, particularly regarding the variation in dose distribution, characterized by maximum deposition at the end of the proton range, known as the distal fall-off of a spread-out Bragg peak. This variation is critical for nearby organs at risk. In this preliminary study, we evaluated the effects of proton irradiation on the neuronal cell population in mouse spinal cord by comparing two positions of the particle range dose deposition profile. We irradiated the spinal cords at the entrance and the distal edge of the spread-out Bragg peak with a single proton dose. Results showed changes in the expression of synaptophysin, a presynaptic protein crucial for synaptic plasticity. Our findings suggest that examining early radiation-induced physiopathological effects on late-responding tissues can provide valuable insights into neuronal plasticity, informing clinical treatment planning for proton beam positioning.

Keywords Synaptic plasticity, RBE, Radiation-induced off-target effects, Proton therapy, Bragg peak

Proton therapy (PT) is a promising strategy to treat radioresistant tumors which are located near organs at risk, such as head and neck tumors, brain, spine and sacrum tumors[1]. The gainful properties of PT fall within the physical rationale of protons that, as light positive ionizing particles, release a maximum energy at the end of the ion range, in correspondence with the so-called Bragg peak, from which it follows with a sudden dose deposition drop[2]. This unique ballistic dose distribution profile allows the increase of the dose delivered on the tumor target, sparing the surrounding healthy organs[3]. However, despite these useful and promising features that have contributed to an incremental expansion of proton use worldwide, PT approaches remain limited and their clinical benefit needs to be further investigated[4]. Less is known about the percentage of patients who may benefit from PT and expert opinions vary significantly[5]. Indeed, is crucial to consider the impact of uncertainties in linear energy transfer (LET), as addressing the relative biological effectiveness (RBE), of PT remains an unresolved issue[6]. Several researches in this field demonstrated that protons energy deposition undergoes a marked increase in LET towards the end of the SOBP, leading to enhanced RBE, defined as the ratio of the absorbed dose of the photon radiation as reference to the absorbed dose of the tested proton radiation, leading to the same biological endpoint[6,7]. The comparison of PT to photon-based treatments faces significant challenges, related to treatment costs and the limited number of operational charged-particle radiation therapy centers. Most of the available data come from non-randomized retrospective studies, which are subject to inevitable

[1]Department of Medicine and Surgery, Kore University of Enna, 94100 Enna, Italy. [2]Institute of Bioimaging and Complex Biological Systems, National Research Council, 90015 Cefalù, Italy. [3]National Institute for Nuclear Physics, Laboratori Nazionali del Sud, 95123 Catania, Italy. [4]Department of Biomedical and Biotechnological Sciences, University of Catania, 95123 Catania, Italy. [5]National Institute for Nuclear Physics, Trento Institute for Fundamental Physics and Applications, 38123 Trento, Italy. [6]Department of Radiation Oncology, University Medical Centre Groningen (UMCG), Groningen, The Netherlands. [7]These authors jointly supervised this work: Giorgio Russo and Rosalba Parenti. ✉email: francescopaolo.cammarata@cnr.it

misclassification and selection biases[8]. While there is broad consensus that the current practice of applying a fixed RBE of 1.1 is inadequate for preventing adverse side effects and accurately predicting patient outcomes, there is no straightforward relationship between dose and clinical outcomes, especially for head and neck and skull-base tumors[7,9]. Clinical prescription doses and dose constraints are largely determined empirically. PT tumor prescriptions and organ constraints are typically based on the physical dose multiplied by a generic constant RBE of 1.1. As protons decelerate, their LET increases, leading to a rise in RBE with depth along a pristine Bragg curve or spread-out Bragg peak (SOBP)[10]. These energy fluctuation values results in an RBE underestimation at the distal part of Bragg peak, which in turn would lead to an over-dosage in the adjacent healthy tissues[11]. This critical issue can contribute to radiation-induced off target effects in late-responding tissues, such as the spinal cord including myelopathy[12]. In our previous study, we examined the early damage after (PT) in the spinal cords of an in vivo model in the distal edge of the *spread-out Bragg peak* (SOBP), reporting evidence of significant insurgence of skin injury[13].

The aim of the present work is to better elucidate the biological effects induced along the Bragg curve, investigating additional deterministic effects on late-responding tissues comparing the entrance of the pristine Bragg peak (LET = 1,10 keV/μM) and the distal edge of the SOBP (LET = 16–18 keV/μM), with a single dose of protons delivered to the mice spinal cord. Since the onset and severity of radiation-induced impairment have been associated to changes in the physiological properties of irradiated neurons, we focused on acute effects occurring in neuron status and synaptic plasticity alteration 2 weeks after irradiation. Our findings indicated the absence of a dose–response increase of neuronal damage, coupled with no significant differences related to the position of the proton beam. However, significant changes in synaptophysin (SYP) expression were found comparing entrance versus distal irradiation. Although the study does not allow definitive conclusions to be drawn, the changes in SYP between entrance and distal at a dose of 19 Gy may be an indication of a physiologicalpatho event that deserves further investigation. These preliminary findings may corroborate the importance of exploring early radiation-induced effects for the assessment of proton beam treatments in different positions along the Bragg curve.

Materials and methods

Ethics statement

The experiments were performed in line with the European Communities Council directive and Italian regulations (EEC Council 2010/63/EU and Italian D.Lgs. 26/2014). The project was approved by Italian Ministry of Health (n. 248/2018-PR of 30/03/2018). All methods were performed in accordance with the relevant guidelines and regulations. The study was carried out in compliance with the ARRIVE guidelines (https://arriveguidelines.org). Efforts were employed to replace, reduce and refine the use of laboratory animals, avoiding the most painful procedures. Mice were monitored at least twice a week for the duration of the experiments; we did not observe any signs of general suffering such as restlessness, mobility loss, grooming failure, open sores, cataracts, and appetite loss until the sacrifice (14 days after irradiation).

Animal models

For this study, C57BL/6 male mice (Charles River Laboratory), 6-week-old were purchased. We waited 1 week for their adaptation in the Center for Advanced in vivo Preclinical Research (CAPiR, University of Catania) animal facility where mice were initially hosted; then mice were transferred to the National Institute of Nuclear Physics (INFN—Laboratori Nazionali del Sud, Catania) animal facility where we waited 1 week for their adaptation. Irradiation was performed on 8-weeks-old mice weighing 25.0 ± 1.4. Two weeks after irradiation, 10-weeks-old mice weighing 27.0 ± 3 were sacrificed for the collection of biological samples. Animals were housed in IVC-cages for 9 weeks using a stocking density of maximum 4 mice per cage. Animals were fed ad libitum and maintained in the same room under a 12:12-h light/dark photoperiod at 24 °C. To minimize suffering and distress of mice, standard environmental enrichment of nest paper, a cardboard fun tunnel and one wooden chew block were provided[13]. A total number of 24 animals was used in this study. Mice were randomly assigned to sham-control group (n = 6) and proton-treated group (n = 18). Each proton-treated group was separated into 2 subgroups of 3 animals: entrance and as follows: 12 Gy entrance (n = 3); 12 Gy distal (n = 3); 15 Gy entrance (n = 3); 15 Gy distal (n = 3); 19 Gy entrance (n = 3) and 19 Gy distal (n = 3). Therefore, for each biological assay, 3 spinal cord samples per subgroups were collected. Technical replicates were analyzed from each spinal cord sample. Each spinal cord sample was divided into two parts. One part was used for Western Blot analysis and the other for immunohistochemistry/immunofluorescence analysis.

Before each irradiation, the mice were anesthetized with Zoletil (tiletamine) 40 mg/kg and Sedastart (medetomidine) 50 μg/kg and shaved in the treatment region. Mice were sacrificed at days 14 post irradiation, after which spinal cord samples were dissected out, cryoprotected and embedded in optimal cutting temperature (OCT) compound. Samples were cut with a cryostat and 20 μm-thick axial sections were mounted on slides and stored at − 20 °C until use as described previously[14].

Dosimetry and proton irradiation setting

All proton experiments were conducted at the Centro di Adroterapia ed Applicazioni Nucleari Avanzate (CATANA) of National Institute of Nuclear Physics—Laboratory of South (INFN-LNS, Catania Italy), utilizing a passive proton beam line. This facility features a fixed horizontal beamline, equipped to deliver clinical proton beams with a maximum energy of 62 MeV. A beam shaping mechanism is utilized to ensure a uniform dose distribution at the isocenter. Along its trajectory, the proton beam come across various elements designed to ensure a flat transverse dose distribution at the isocenter, as have been appropriately described in previous works[15].

To ensure precise and reproducible mice position, a dedicated animal holder system was utilized, and a range shift was employed to accurately position the animal's target. Adjustment of field size was achieved using a custom-made collimator crafted from 6.3 mm thick brass, featuring a rectangular aperture measuring 10 × 25 mm. The heterogeneity of the lateral beam measured at the irradiation isocenter was below 2%. Prior to irradiation, verification of beam flatness was conducted utilizing a motorized silicon detector. Moreover, a polymethyl methacrylate (PMMA) modulator wheel was employed to generate a Spread-Out Bragg Peak (SOBP) with a plateau width of 14.8 mm and a practical range extending to 30.2 mm.

Dosimetry procedures involved the use of Markus ionization chamber (PTW Freiburg GmbH, Germany) and Gafchromic EBT3 films (ISP Corp., New York, USA). For each irradiation session, the beam flatness and the dose release were assessed positioning a Gafchromic EBT3 film before the target. At 24 h post-irradiation, the films were scanned using an Epson Expression 10,000 XL Scanner (Epson, Germany) and evaluated with a custom MatlabTM script.

Dose delivery monitoring was achieved through a transmission ionization chamber across the beam line, which automatically ceased beam emission upon reaching the designated number of monitor units (MU). MU calibration, correlated with absolute dose to water, was determined through measurements using the Advanced Markus IC at the midpoint of SOBP position. Specifically, all irradiation procedures were performed at a steady dose rate of 5 Gy/min.

Monte Carlo (MC) simulation is commonly used in clinical settings for its ability to predict dose distribution accurately and efficiently within the target area. This tool is particularly valuable for irradiating small animals due to their smaller dimensions. In this context, the application developed by our team facilitates the simulation of in vivo studies conducted in the CATANA experimental room, integrating the possibility to improve the target analysis through the DICOM microCT images[13]. In addition, this application allows for the simulation of beam interaction with the real geometry of small animals. The simulation employs the QGSP_BIC models for hadronic processes and the G4EmStandardPhysics option4 for electromagnetic processes, recommended for proton energies below 200 MeV/A. The application was utilized to design the irradiation setup, determine suitable combinations of modulator wheel and range shifter for accurate target positioning along the SOBP, and calculate dose distributions and LET values within the target.

For the irradiation of anesthetized mice, two experimental setups were defined: one referred to as "entrance", which involved the use of a pristine Bragg peak (Fig. 1a), and the second using a SOBP referred to as "distal", (Fig. 1b). In the "entrance" configuration, the mice were positioned with their sides facing the nozzle, with the spinal cord perpendicular to the beam, such that only the entrance of the beam (LET 1.1 keV/μm) delivered its dose to the spinal cord, thus avoiding further penetration of the beam into the animal and additional dose release to other organs and tissues. In the "distal" configuration, mice were positioned with their backs facing the nozzle, allowing irradiation of the spinal cord with the distal part of the Bragg peak (LET 16–18 keV/μm) (Fig. 1a,b). In our irradiation setting we ensured that the curved lumbar portion of the spinal cord was irradiated. To do this we appropriately sheared the mice in the area of interest, framed with the light field of the CATANA beam system (Supplementary Fig. 2).

Immunohistochemistry and immunofluorescence

Samples were collected by performing hydraulic spinal cord extrusion. Firstly, we performed euthanasia using isoflurane and CO_2 to avoid any signs of pain and suffer for the animals. Before the extrusion of the spinal cord, we isolated the spinal cord cutting along the spinal column in a distal direction past the pelvic bone. Then, we trim the spinal column with scissors to ensure that it was visible at both ends. For spinal cord extraction we used a 5 mL syringe, replacing the needle with a 2–200 μM tip, specially cut to fit the syringe. To extrude the spinal cord we applied constant pressure until the sample settled on the Petri dish kept on ice. Samples were then washed in PBS and the lumbar portions were taken, which were exposed to the proton beam. Each portion was divided into two parts, one of which was snap frozen for protein extraction and the other was post-fixed in 4% PFA in PBS at 4 °C overnight. Fixed samples for cryosectioning were left for at least 48–72 h in 30% sucrose in PBS at 4 °C for cryo-protection. Finally, they were embedded in optimum cutting temperature (OCT) medium, frozen with liquid nitrogen and 20 μm cryo-sectioning was performed. For Cresyl Violet Staining, sample slides were de-hydrated with increasing concentration of ethanol (70%, 95%, 95%, 100%, 3 min each) and then in xylene, and re-hydrated using decreasing concentration of ethanol in water (100%, 95%, 70%, 3 min each) and then water. For quantification of motoneurons (MNs) sections were stained with cresyl violet, coverslipped and acquired using a Nexcope NIB600 biological microscope microscope, and analysed using ImageJ software (NIH, Bethesda, MD, USA). The number of MNs was obtained from the left and right side of the spinal cord. In all counts, only cell profiles with unambiguous motoneuronal morphology and size were considered. Sections were subjected to a protocol of antigen retrieval heating (5 min × 3) in capped polypropylene slide-holders with citrate buffer (0.1% Tween 20 in citrate buffer solution), using a microwave (5 min per 3 cycle, 440 W). To reduce non-specific immunoreactivity samples were incubated for 30 min in 0.3% H_2O_2 to quench endogenous peroxidase activity for 15 min at room temperature. Slides were then washed in PBS, then incubated for 1 h with rabbit polyclonal anti-cleaved caspase-3 antibody (Cell Signalling Technology Cat#9661, RRID:AB_2341188). Then, samples were washed in 0.3% Triton in PBS 3 times for 5 min and samples were incubated with biotinylated secondary antibody, diluted in PBS containing 1% bovine serum albumin (Horse Anti-Mouse/Rabbit/Goat IgG Antibody (H + L), Cat# BA-1300, RRID: AB_2336188, 1:200) for 30 min at room temperature. After a 5 min washing, slides were incubated with avidin–biotin–peroxidase complex (VECTASTAIN Elite ABC-HRP Reagent, Vector Laboratories, Cat# PK-7100) for 30 min at room temperature. The immunoreaction was visualized by incubating the sections for 4 min in a 1% 3,30-diaminobenzidine (DAB) and 0.3% hydrogen peroxide solution in PBS. Nuclei were counterstained with Mayer's hematoxylin (Sigma-Aldrich, Cat# MHS32). Slides were then dehydrated using a series of increasing ethanol concentrations (50%, 70%, 95%, 100%) and cleared with

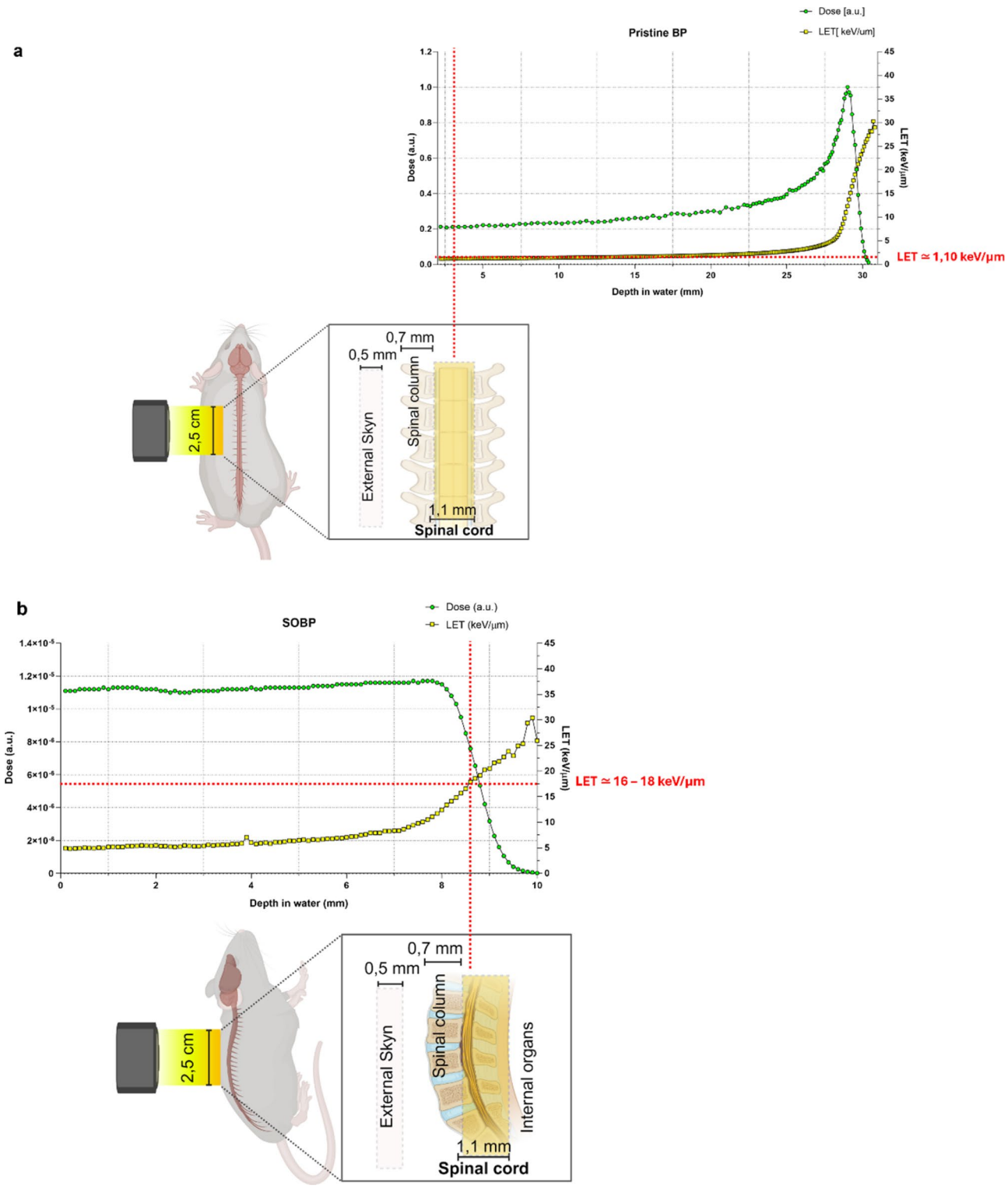

Fig. 1. Experimental irradiation setup used for the "entrance" (low LET) and the "distal" (high LET) configuration. Mice positioned at the "entrance" had their sides facing the nozzle, with the spinal cord perpendicular to the beam, such that only the entrance of the beam (LET 1.1 keV/µm) delivered its dose to the spinal cord, thus avoiding further dose release to other tissues (**a**). In the "distal" configuration, mice were positioned with their backs facing the nozzle, allowing irradiation of the spinal cord with the distal part of the Bragg peak (LET 16–18 keV/µm) (**b**). Created with BioRender.com.

xylene. Finally sections were mounted using Eukitt mounting medium (Bio Optica, Cat# 09-00250). Pictures were acquired using the Nexcope NIB600 biological microscope. For cleaved caspase 3 quantification, staining intensity score was graded on a 0–3 scale, according to the following assessments: no detectable staining = 0, weak staining = 1, moderate staining = 2, strong staining = 3[16].

To investigate colocalized synaptophysin on neuron, slides were washed in 0.3% Triton X-100 in PBS, 2 times for 5 min at room temperature. Then sections were blocked with blocking solution of 10% normal goat serum (NGS) for 1 h at room temperature in a humidity chamber. Sections were labelled with mouse anti-SYP (Santa Cruz Biotechnolgies, Milan, Italy; Cat.#sc-9116; RRID:AB_2199007; dilution: 1:100) and Mouse anti-Neuronal nuclear antigen (NeuN) (Abcam; Cat.#: ab104224; RRID:AB_ 10711040; dilution: 1:300) with 1% NGS in 0.3% Triton X-100 in PBS. On the following day, after 3 washes with 0.3% Triton X-100 in PBS, slides were incubated for 1 h at room temperature with the appropriate secondary antibodies: goat polyclonal anti-mouse (Alexa Fluor 546 Thermo Fisher Scientific, Cat#A-11003, RRID: AB_2534071, dilution 1:1,000) and goat polyclonal anti-rabbit (Alexa Fluor 488, Thermo Fisher Scientific, Cat#A-11008, RRID: AB_143165). Nuclei were counterstained with 4,6-diamidino-2-phenylindole (Dapi, Invitrogen, Cat.#: D1306; dilution: 1:1,000) for 3 min at room temperature and then mounted with Fluoromount Aqueous Mounting Medium (Sigma-Aldrich, Cat.#: F4680). Digital images were acquired and quantified using a Leica TCS SP8 confocal microscope. For quantification of synaptophysin mean fluorescence intensity (MFI), and mature neuronal marker NeuN colocalization $n \geq 5$ regions of interest per $n \geq 3$ sections per animal were analysed and quantified by operators blinded to the treatment using ImageJ v. 2.1.0/1.53c (Fiji) software.

For motoneurons quantifications we focused on the ventral horn of the grey matter from both sides on the region, where sciatic motor pool is clustered. Otherwise, the quantification of cleaved caspase-3 was obtained from $n \geq 3$ spinal cord ROIs from each section and the average was calculated. Three slides from $n = 3$ independent replicates per condition were quantified and calculated as mean numbers (± SEM).

Immunoblotting

Freshly isolated spinal cord biopsies were homogenized with 1 × RIPA lysis buffer (10 µL/mg tissue; abcam, Cambridge, UK), supplemented with a cocktail of protease inhibitors (Sigma-Aldrich s.r.l., Milano, Italy), as previously described[17,18]. Briefly, samples were incubated for 20 min at room temperature, sonicated (5 cycles/30 s), and centrifuged at 13,000 × g for 5 min. Supernatants were collected and stored at − 80 °C until use. The extracted proteins were quantified using a Multiskan SkyHigh Microplate spectrophotometer (Thermo Scientific). Protein samples containing an equal amount of proteins (20 µg) were electrophoresed on 4–20% SDS-PAGE gels and transferred to nitrocellulose membranes. Membranes were incubated for 1 h at room temperature with blocking buffer (5% non-fat milk in 0.1% tween-20 in PBS) and then overnight at 4 °C with primary antibodies diluted in blocking buffer. The following primary antibodies were used for immunoblotting: mouse anti-SYP (Santa Cruz Biotechnologies, Milan, Italy; Cat.#: sc-17750; RRID:AB_628311 dilution: 1:500), and rabbit anti-GAPDH (Abcam; Cat.#ab181602; RRID:AB_2630358 dilution: 1:3000). Then, membranes were washed 3 times in 0.1% tween-20 in PBS and then incubated for 1 h at room temperature with the appropriate secondary antibody: Goat anti-mouse (Invitrogen Cat.#: 31430; RRID:AB_228307 dilution: 1:5000) or goat anti-rabbit (Invitrogen; Cat.#31460; RRID:AB_228341dilution: 1:10′000) HRP-conjugated. Proteins bands were detected using SuperSignal™ West Pico PLUS Chemiluminescent Substrate (Thermo Scientific) according to the manufacturer's instructions and revealed with the ChemiDoc System (Bio-Rad). The density of each band was quantified using ImageJ v. 2.1.0/1.53c (Fiji) software analysis software and the band density was normalized to the GAPDH optical density measured in the same membrane. As previously explained, each experimental subgroup consists of 3 spinal cord samples which are considered 3 independent replicates. Western blot proteins were extracted from each spinal cord generating $n = 2$ technical replicates. The technical replicates of each independent sample were quantified obtaining values that were normalized versus GAPDH. For each technical replicates the fold change was calculated over the normalized values of the control group.

Statistical analysis

Data analysis was performed using GraphPad Prism software version 5.0.1. Data were tested for normality using a Shapiro–Wilk normality test and subsequently assessed for homogeneity of variance. Data that passed both tests were further analysed by two-way ANOVA comparing $n > 2$ groups with Holm–Sidak post-hoc test for multiple comparisons were used where appropriate . Data are presented as the mean ± standard error of the mean (SEM). A value of $p < 0.05$ was considered statistically significant and symbols used to indicate statistical differences are described in figure legends.

Results

Proton irradiation induced an increase in spinal cord cell damage at the beam entrance and distal position

We first evaluated the effect of entrance versus distal edge of SOBP proton irradiation on lamina IX resident spinal motoneuron (MN) population. We reported a depletion trend of MNs from 12 to 19 Gy but no significant differences were observed in the entrance as compared to the distal irradiated mice spinal cord (Fig. 2a–e).

We then moved to analyze pro-apoptotic signaling via immunohistochemical-assisted analysis on lamina IX cell populations of the spinal cord. Sections were stained with the apoptotic marker cleaved caspase-3 and our analysis revealed a significantly higher intensity score in irradiated mice with 19 Gy, both for entrance and distal, as compared to sham irradiated group. We did not find any significant changes of intensity relative score between the entrance and the distal irradiated subgroup at the same doses (Fig. 3a–e). Furthermore, the apoptosis signal was significantly increased in spinal cord samples irradiated with 19 Gy at distal compared to the 12 Gy group. There were no significant differences between 15 and 19 Gy irradiated groups.

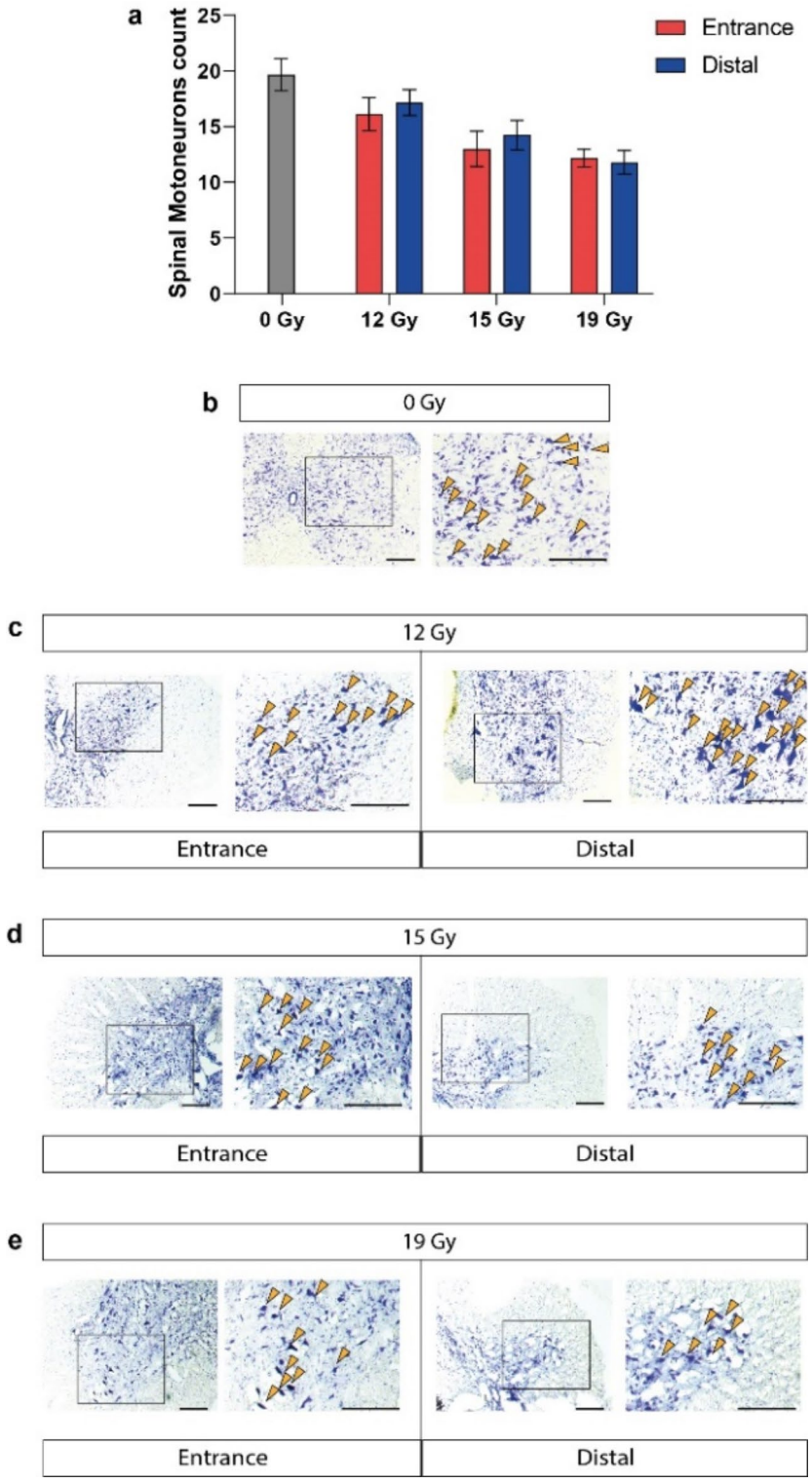

Fig. 2. Evaluation of motoneurons following proton irradiation. Quantification of the number of motoneurons after proton irradiation (**a**) and representative pictures of spinal cord lamina IX stained with cresyl violet after proton irradiation at entrance and distal positions (yellow arrows for motoneurons) (**b**, **c**, **d**, **e**). Data are plotted by interleaved bars with mean ± SEM of n = 6 mice for sham irradiated group and n = 3 mice for treated subgroups. Statistical analysis was performed using two-way ANOVA; scale bars: 200 µm.

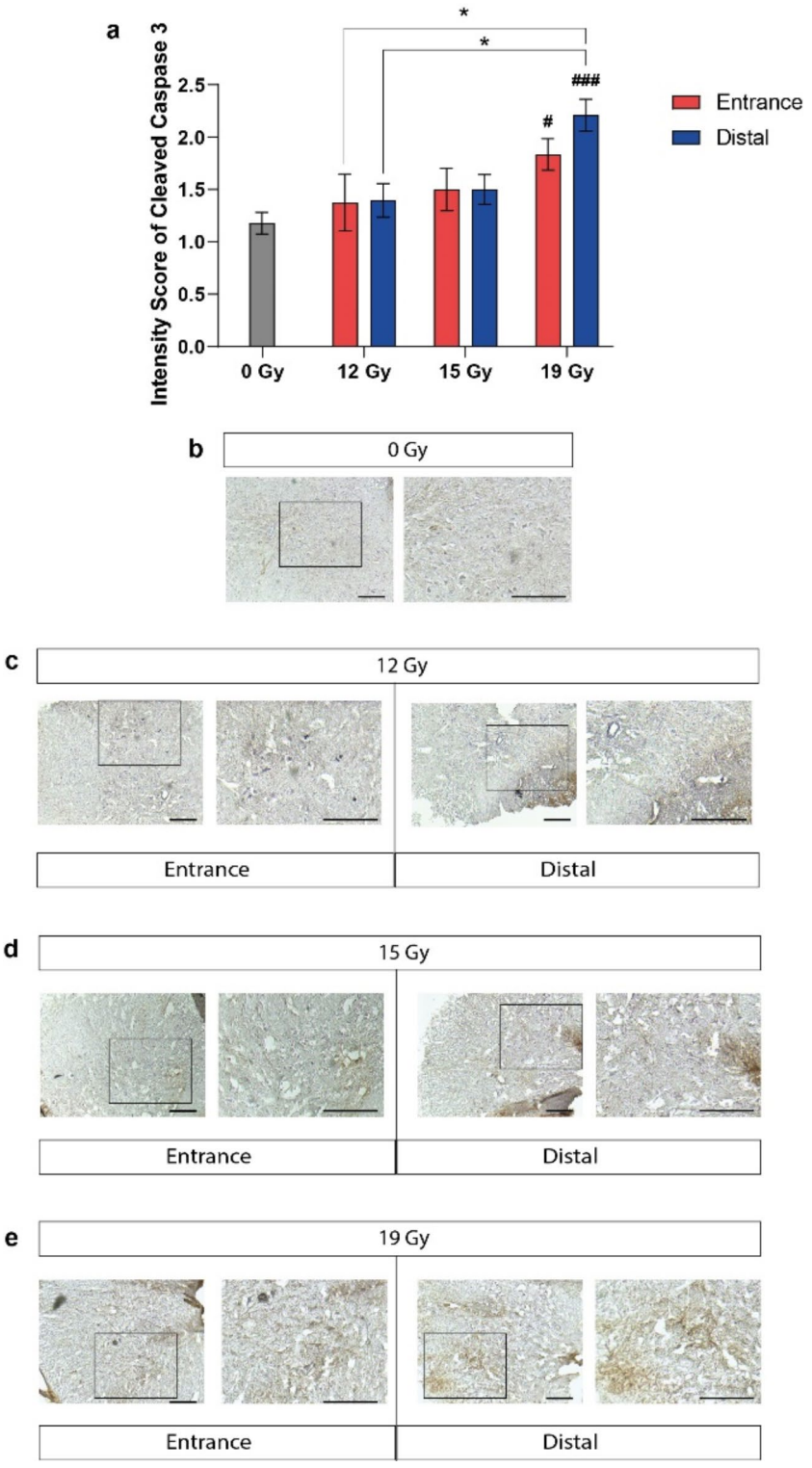

Fig. 3. Evaluation of apoptosis in spinal cord neurons following proton irradiation. Quantification of the intensity relative score of Cleaved Caspase-3 on proton irradiated spinal cord (**a**) and representative pictures of spinal cord sections stained for Cleaved Caspase-3 after proton irradiation at entrance and distal positions (**b, c, d, e**). Data are plotted by interleaved bars with mean ± SEM of n = 6 mice for sham irradiated group and n = 3 mice for treated subgroup. Statistical analysis was performed using two-way ANOVA; #*p*-value < 0.05 and ###*p*-value < 0.001 05 versus 0 Gy; **p*-value < 0.05 between groups; scale bars: 200 µm.

Therefore, these results suggested that proton irradiation induced an increase of early damage with an escalation dose ranging from 12 to 19 Gy, affecting the survival capability of spinal cord resident cell population in a dose dependent way, regardless the position along the Bragg peak.

Evaluation of neuronal plasticity biomarkers after proton irradiation at the beam entrance and distal position

Given the absence of significant differences between entrance and distal on the proportion of spared MNs and on the pro-apoptotic signaling, we aimed at investigating the involvement of synaptic plasticity processes. Thus, we focused our analysis on the expression of SYP, which is a key factor for neuron growth and differentiation, acting at the pre-synaptic site. We found that 12 Gy and 15 Gy of proton irradiation at both positions, determined an increased expression of SYP as compared to 0 Gy (Fig. 4a,b). The increase in SYP expression levels was also maintained at 19 Gy, but only for the distal position (Fig. 4a,b). From a comparison between the entrance and distal positions at the same doses, we reported that only proton irradiation at the distal position for 19 Gy dose, resulted in a significant increase in expression levels of SYP (Fig. 4a,b).

From the multiple comparison between all doses, it has been observed that SYP expression at either entrance or distal 12 Gy doses were lower than that at entrance or distal 15 Gy and distal 19 Gy subgroups (Fig. 4a,b). The highest expression levels of SYP occurred on entrance 15 Gy dose irradiated mice spinal cords, which was also higher than that at distal 19 Gy subgroup, whereas the irradiation of distal 15 Gy dose was higher than entrance 19 Gy subgroup, but of a similar magnitude as compared to distal 19 Gy dose (Fig. 4a,b).

Taken together we can summarize our evidence refereed to the presynaptic protein SYP, reporting on increased level along the dose at 12 Gy and 15 Gy for both positions, lowering at entrance 19 Gy dose.

Given the dose-dependent increase of SYP in the spinal cord and the following reduction at entrance 19 Gy dose irradiated mice, we further investigated SYP in association with NeuN, as marker of neuronal plasticity. We performed a confocal-assisted analysis at the highest irradiation dose of 19 Gy comparing entrance versus distal; we decided to focus our attention on this dose, since it was the only that reported a significative difference of SYP expression between the entrance and the distal position. From quantifications of immunofluorescence images, we reported that 19 Gy irradiation of the mice spinal cords in both positions resulted in a decreased level of NeuN MFI (Fig. 5a,c). On the other hand, qualitative analysis of the sections showed NeuN in neurons at the nuclear and/or perinuclear level and a roughly diffuse SYP signal due to the axonal terminals maintaining contacts with the resident MN population. For this reason, in order to obtain a specific background signal-independent measurement, we decided to measure MFI of colocalized SYP with NeuN, expressed as SYP to NeuN ratio MFI. At the distal and entrance positions there were no significant changes of SYP as compared to the sham irradiated. However, SYP was found increased in samples treated with 19 Gy at the distal as compared to the entrance (Fig. 5b,c).

Discussion

In recent years, particle therapy research has achieved positive insights into the specific mechanisms of radiation damage. Several efforts have been made to combine basic physics and radiobiology research to advance therapeutic approaches. Among the several radiobiological parameters which are subject of study in particle therapy, the RBE is certainly one of the most discussed issues. Indeed, several years of debate are running about its use in the case of protons, which could increase as a function of LET, from the entrance to the distal fall-off

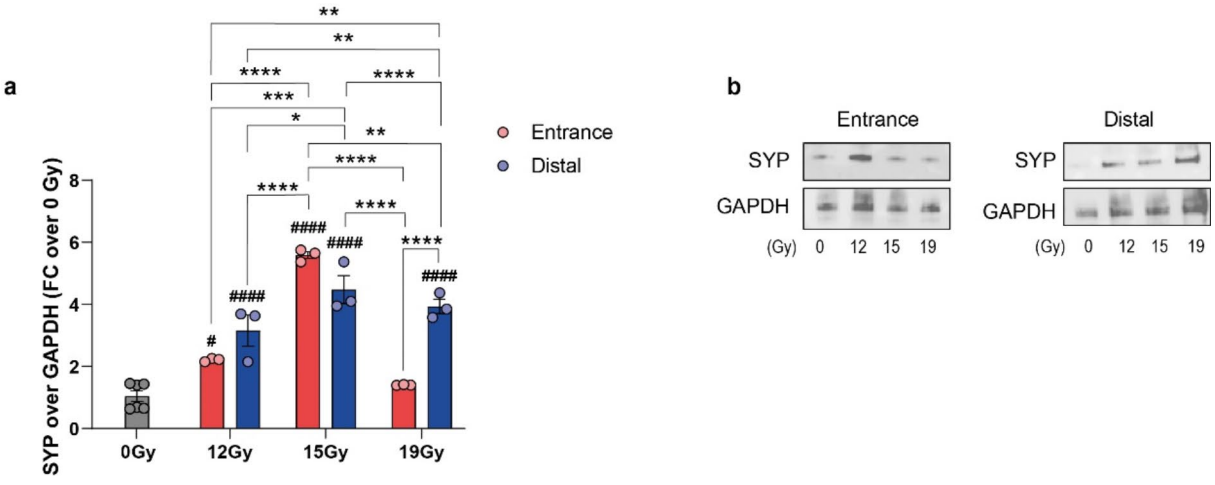

Fig. 4. Evaluation of SYP expression analysis. Quantification of western blot analysis for SYP (**a**), and representative blots of spinal cord samples exposed to proton irradiation at 0 Gy, 12 Gy, 15 Gy and 19 Gy at the entrance and distal position of Bragg Peak (**b**). Statistical analysis was performed using two-way ANOVA. Data are expressed as mean ± SEM of n = 3 independent experiments. FC, fold change; ####p-value < 0.0001 and ###p-value < 0.001 versus 0 Gy; ****$p < 0.0001$, ***$p < 0.001$, **$p < 0.01$ and *p-value < 0.05 versus entrance at the same dose or between groups. The original blots/gels are presented in Supplementary Fig. 1.

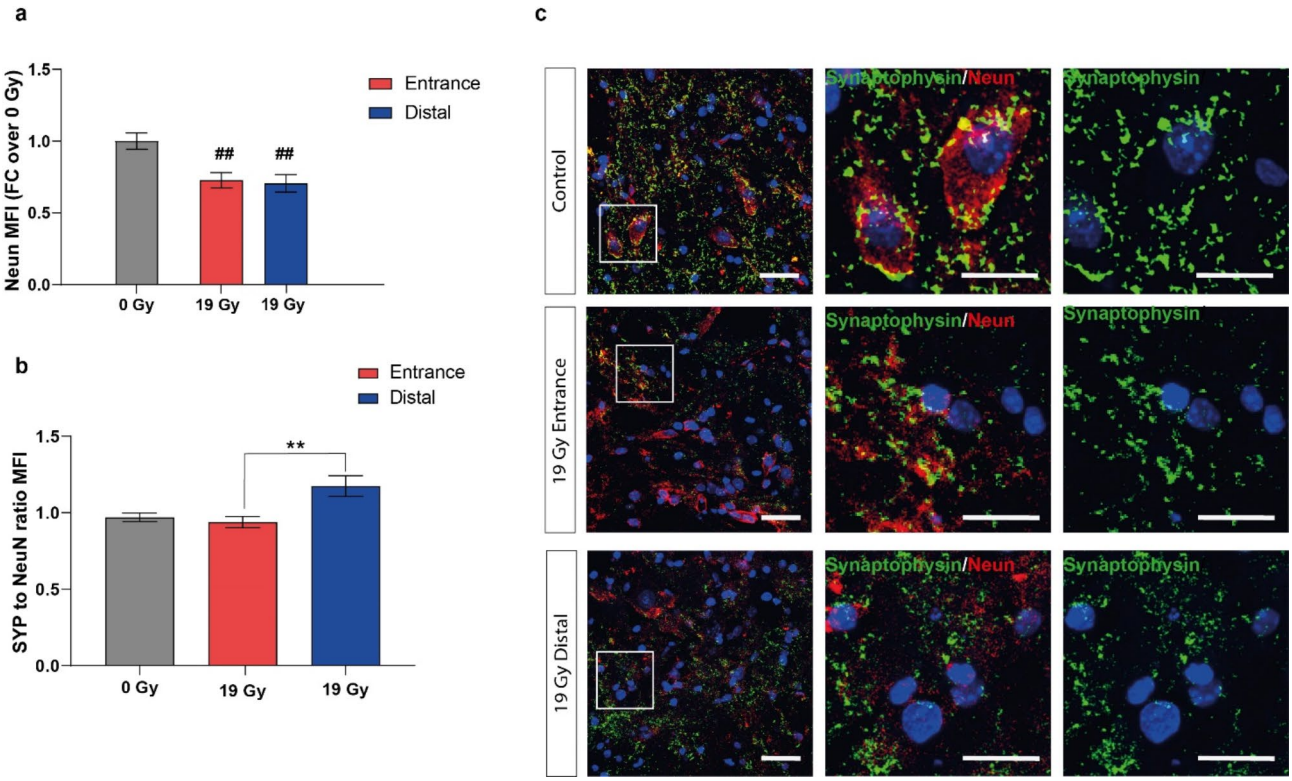

Fig. 5. Evaluation of NeuN and SYP colocalization with NeuN. Quantification of NeuN MFI (**a**) and SYP to NeuN ratio MFI (**b**). Representative pictures of NeuN and SYP immunofluorescence on irradiated spinal cord with 0 Gy and 19 Gy of protons entrance and distal (**c**); scale bars: 100 µm (full images) and 50 µm (region of interest). Statistical analysis was performed using two-way ANOVA. Data are plotted by interleaved bars with mean ± SEM of n = 6 mice per sham irradiated and n = 3 mice per treated subgroups. ##$p < 0.01$ versus 0 Gy and **$p < 0.01$ between groups.

of SOBP. Even though supported by several studies, it is still not clear whether and how the dose delivered can be critical for close-by organs at risk.

The objective of the present study was to investigate cellular and molecular processes that could be involved in radiation-induced transient myelopathy and the more serious chronic progressive myelopathy, comparing the typical low LET of the entrance with the high LET of SOPB proton irradiation after 2 weeks, in order to assess the early effect on resident neuronal cell population. In the first part of the study, the survival of the neurons was evaluated. A trend of reduction of motor neurons with increasing dose was reported but no significant differences emerged in relation to the position of the proton beam. The analysis was deepened by evaluating spinal pro-apoptotic signaling, finding that irradiation at 19 Gy determined higher increase in the apoptotic signal as compared to sham irradiated, but once again the distal position did not have a different impact versus the entrance. Thus, the study focused on processes involved in neuronal maturation and synaptic plasticity. Therefore, we analyzed the presynaptic protein SYP, whose expression levels increased along the dose, peaking at 15 Gy, and with significantly higher levels maintained on distal 19 Gy dose subgroup.

To deepen the study on SYP at 19 Gy, an immunofluorescence investigation was carried out coupling SYP and the neuronal marker NeuN. While NeuN was decreased in the 19 Gy treatment, no differences were reported for SYP between 19 Gy versus the sham irradiated group. However, a significant difference emerged between the 2 positions of the proton beam.

A previous study evaluated the post-synaptic density protein (PSD-95) in addition to SYP, following proton irradiation[19]. It was used a low dose of whole-body proton irradiation at a single peak position. It was highlighted that irradiated hippocampal neurons showed a significant and persistent reduction in SYP levels after 10 and 30 days of irradiation, while the PSD-95 expression significantly increased at the same time points compared to controls. Previous studies have focused on evaluating the RBE of protons along the Bragg peak studying long-term effects such as myelopathy. In one of this, RBE of protons as a function LET and dose was tested in the rat spinal cord, with single or two equal fractions of protons at four positions (LET 1.4–5.5 keV/mm) along a 6 cm SOBP[20]. The authors reported a moderate increase of RBE at the distal edge of the proton SOBP. An even more recent study calculated RBE using single and multi-fraction entrance and Bragg peak proton beam, monitored over 1 year for changes in weight, mobility, and general health, with radiation-induced myelopathy as the primary biological endpoint[12]. In this study it has been demonstrated that RBE can vary as much as 25% when comparing the first part of the curve with the peak portions of the Bragg curve[12].

Despite the potential advantages of PT, particularly for the central nervous system, there is limited or no data available on how proton irradiation affects the intricate neuronal subcellular structures. This gap in knowledge becomes even more pronounced when considering the effects of varying LET within the Bragg peak region. While previous studies on myelopathy have primarily focused on the long-term motor deficits, little is understood about the immediate biological mechanisms following PT exposure. This preliminary study shows a first pathophysiological analysis, highlighting the need to investigate early cellular and molecular processes within the nervous system, which may serve as precursors to pathological manifestations linked to LET differences.

Other studies for early damage in vivo irradiation have instead evaluated skin damage, but few studies have compared the effects of RBE of protons in relation to LET. Among these, a previous study applied a dose plan of 4 mm intervals from the middle of the SOBP to behind the distal dose fall-off, reporting an enlarged skin damage with the increased LET in the distal edge of the SOBP[21].

In conclusion, the data emerging from the most recent studies on LET-dependent radiation damage, are proving increasingly useful for the optimization of particle therapeutic approaches. Our preliminary results, highlighting changes in the expression of a specific pre-synaptic protein, provide a further key to understand the implications useful for the evaluation of synaptic plasticity processes involved in early LET-dependent radiation damage.

This study faces several important limitations that should be acknowledged. First, we only examined a portion of the spinal cord in mice, rather than analyzing the entire structure, which may have led to incomplete data on potential widespread effects. Second, we did not make a detailed comparison between gray and white matter, two critical spinal cord components that may react differently to experimental conditions. Additionally, the study relied on a low number of animal models, which limits the statistical power and generalizability of the findings. Third, while our study focuses on the spinal cord, the biological synaptic plasticity processes identified in the spinal cord may also occur in brain structures, which we did not examine at this stage. Lastly, due to the preliminary nature of this work, the study does not offer a definitive translational message for biomedical applications and should be viewed as a foundation for future and additional experimental research in this field.

Data availability

All data generated or analysed during this study are included in this published article [and its supplementary information files].

Received: 31 May 2024; Accepted: 30 December 2024
Published online: 16 January 2025

References

1. Yuan, T. Z., Zhan, Z. J. & Qian, C. N. New frontiers in proton therapy: Applications in cancers. *Cancer Commun. (Lond)* **39**(1), 61 (2019).
2. Mohan, R. A review of proton therapy—Current status and future directions. *Precis. Radiat. Oncol.* **6**(2), 164–176 (2022).
3. Mohan, R. & Grosshans, D. Proton therapy—Present and future. *Adv. Drug Deliv. Rev.* **109**, 26–44 (2017).
4. Timmermann, B. Editorial: Proton therapy in cancer treatment: clinical evidence and controversies. *Front. Oncol.* **11**, 791302 (2021).
5. Burnet, N. G. et al. Estimating the percentage of patients who might benefit from proton beam therapy instead of X-ray radiotherapy. *Br. J. Radiol.* **95**(1133), 20211175 (2022).
6. Paganetti, H. Proton relative biological effectiveness—Uncertainties and opportunities. *Int. J. Part. Ther.* **5**(1), 2–14 (2018).
7. Deng, W. et al. A critical review of LET-based intensity-modulated proton therapy plan evaluation and optimization for head and neck cancer management. *Int. J. Part. Ther.* **8**(1), 36–49 (2021).
8. Chen, Z. et al. Proton versus photon radiation therapy: A clinical review. *Front. Oncol.* **13**, 1133909 (2023).
9. Holtzman, A. L. et al. Impact of relative biologic effectiveness for proton therapy for head and neck and skull-base tumors: A technical and clinical review. *Cancers (Basel)* **16**(11), 1947 (2024).
10. Paganetti, H. Relative biological effectiveness (RBE) values for proton beam therapy. Variations as a function of biological endpoint, dose, and linear energy transfer. *Phys. Med. Biol.* **59**(22), 419–72 (2014).
11. Byun, H. K. et al. Physical and biological characteristics of particle therapy for oncologists. *Cancer Res. Treat* **53**(3), 611–620 (2021).
12. Denbeigh, J. M. et al. Characterizing proton-induced biological effects in a mouse spinal cord model: A comparison of bragg peak and entrance beam response in single and fractionated exposures. *Int. J. Radiat. Oncol. Biol. Phys.* **119**, 924–935 (2024).
13. Pisciotta, P. et al. Evaluation of proton beam radiation-induced skin injury in a murine model using a clinical SOBP. *PLoS One* **15**(5), e0233258 (2020).
14. Vicario, N. et al. Clobetasol promotes neuromuscular plasticity in mice after motoneuronal loss via sonic hedgehog signaling, immunomodulation and metabolic rebalancing. *Cell Death Dis.* **12**(7), 625 (2021).
15. Pisciotta, P. et al. Monte Carlo GEANT4-based application for in vivo RBE study using small animals at LNS-INFN preclinical hadrontherapy facility. *Phys. Med.* **54**, 173–178 (2018).
16. Cammarata, F. P. et al. Proton boron capture therapy (PBCT) induces cell death and mitophagy in a heterotopic glioblastoma model. *Commun. Biol.* **6**(1), 388 (2023).
17. Spitale, F. M. et al. Increased expression of connexin 43 in a mouse model of spinal motoneuronal loss. *Aging (Albany NY)* **12**(13), 12598–12608 (2020).
18. D'Aprile, S. et al. Anaplastic thyroid cancer cells reduce CD71 levels to increase iron overload tolerance. *J. Transl. Med.* **21**(1), 780 (2023).
19. Parihar, V. K. et al. Persistent changes in neuronal structure and synaptic plasticity caused by proton irradiation. *Brain Struct. Funct.* **220**(2), 1161–1171 (2015).
20. Saager, M. et al. Determination of the proton RBE in the rat spinal cord: Is there an increase towards the end of the spread-out Bragg peak?. *Radiother. Oncol.* **128**(1), 115–120 (2018).
21. Sorensen, B. S. et al. Relative biological effectiveness (RBE) and distal edge effects of proton radiation on early damage in vivo. *Acta Oncol.* **56**(11), 1387–1391 (2017).

Acknowledgements
The authors would like to thank the Center for Advanced Preclinical in vivo Research (CAPiR) and the confocal microscopy facility at the Bio-Nanotech Research and Innovation Tower (BRIT) of the University of Catania, for the technical contribution of the staff.

Author contributions
The first draft of the manuscript was written by Filippo Torrisi and all authors commented on previous versions of the manuscript. Material preparation, data collection and analysis were performed by F.T., A.M.P., S.D., S.D.A, A.G., C.A., N.V., F.P.C; conceptualization: F.T., F.P.C., N.V., G.R., R.P.; methodology, formal analysis and investigation, F.T., V. B., M.C., G.P., G.A.P., E.S., P.P..resources: G.R., R.P.; samples acquisition and biobanking: F.T., A.M.P., S.D., S.D.A, A.G., C.A.,; data curation, F.T., F.P.C., N.V., G.R., R.P.; all co-authors reviewed the manuscript. All authors have read and agreed to the published version of the manuscript.

Funding
The research was supported by the following grants:1) INFN CSN V—Call "MoVe-IT"; 2) Italian Ministero dell'Istruzione, dell'Università e della Ricerca, PRIN 2017, Grant No.: 2017XKWWK9_004 to R.P. and G.R. This study was also partially funded by the 3) National Plan for NRRP Complementary Investments (PNC, established with the decree-law 6 May 2021, n. 59, converted by law n. 101 of 2021) in the call for the funding of research initiatives for technologies and innovative trajectories in the health and care sectors (Directorial Decree n. 931 of 06-06-2022)—project n. PNC0000003—AdvaNced Technologies for Human-centrEd Medicine (project acronym: ANTHEM) and by the 4) National Recovery and Resilience Plan (NRRP), Mission 4 Component 2 Investment 1.4—Call for tender No. 3138 of 16 December 2021, rectified by Decree n.3175 of 18 December 2021 of Italian Ministry of University and Research funded by the European Union—NextGenerationEU; Award Number: Project code CN_00000033, Concession Decree No. 1034 of 17 June 2022 adopted by the Italian Ministry of University and Research, B83C22002930006, Project title "National Biodiversity Future Center—NBFC".

Declarations

Competing interests
The authors declare no competing interests.

Ethical approval
Approval was granted by the Ethics Committee of University of Catania, Catania (Italy), approval Code: 248/2018-PR of 30/03/2018, according to Ministry of Health. All data generated or analysed during this study are included in this published article [and its supplementary information files].

Additional information
Supplementary Information The online version contains supplementary material available at https://doi.org/10.1038/s41598-024-84902-2.

Correspondence and requests for materials should be addressed to F.P.C.